

# Modeling and Simulation of Enzyme-Catalysed Substrate Conversion in a Microbioreactor

Linas Petkevičius and Romas Baronas

Institute of Computer Science, Vilnius University,  
Didlaukio st. 47, Vilnius, Lithuania

Email: {linas.petkevicius, romas.baronas}@mif.vu.lt

**Abstract**—Mathematical modeling and numerical simulation of non-linear mathematical model for digital simulation of an enzyme loaded porous microreactor is investigated in this paper. The model is based on a system of reaction-diffusion equations, containing a non-linear term related to the Michaelis-Menten kinetics, and involves three regions: the enzyme microreactor where the enzyme reaction as well as mass transport by diffusion take place, a diffusion limiting region (the Nernst layer), where only the mass transport by diffusion takes place, and a convective region, where the constant analyte concentration is maintained. The digital simulation was carried out using the finite difference technique. Assuming well-stirred conditions, impact of the diffusion modulus and the Biot number as well as porosity on transient effectiveness factor and yield factor has been numerically investigated. The simulation results showed that the Nernst layer must be taken into consideration when modelling micro-size bioreactors. The computational simulations showed that the yield factor and the effectiveness factors have different properties to describe system productivity.

**Keywords**—reaction-diffusion; Michaelis - Menten kinetics; microbioreactor; porosity; CSTR.

## I. INTRODUCTION

This paper is an extension of the work originally reported in The Ninth International Conference on Advances in System Simulation [1].

Continuous-flow stirred tank reactors (CSTR) are common in chemical industries [2][3]. Although a stirred tank is a usual construction of industrial enzyme reactors, the effectiveness and optimal construction of CSTR remain open to study [4][5]. Specifically, further research is needed due to the application of the immobilized enzymes, such as biocatalysts, on a manufacturing scale that requires to use the reactors of different types, including CSTR [6][7][8].

The CSTR often refers to the model used to estimate the operation parameters when using a continuous agitated-tank reactor to reach a specified output [7]. In the last few decades, immobilized enzyme reactor models have evolved significantly with a wide range of applications in food industry [9], waste cleaning [10], immobilization of microbial cells [11][12]. The main advantages of immobilized cells over non-immobilized cells can be enumerated: (1) incapsulation not only keep enzyme from wash out, but also protect it during the changes of various conditions, such as pH, temperature, and toxic compounds; (2) cells do not stick up to bioreactors

or other materials within the reactor; (3) reusability; and (4) control over reactions that are allowed, shell can be formatted to avoid the diffusion of all material to microreactor. Rapid progress was noticed in integrating microfluidic reactors and biocatalytic reactions [13]. The combination of miniaturized technologies and microfluidics allows to increase the efficiency of bioprocess. In the recent review, Jansen concludes that end-to-end fabrication and on-demand manufacturing based on microreactors have growing industrial interest, which leads to development and progress [14]. However, coupling microreactors and biocatalysis is highly complex, requiring an integrated approach addressing biocatalyst features, reaction kinetics, mass transfer and microreactors geometry [13][15].

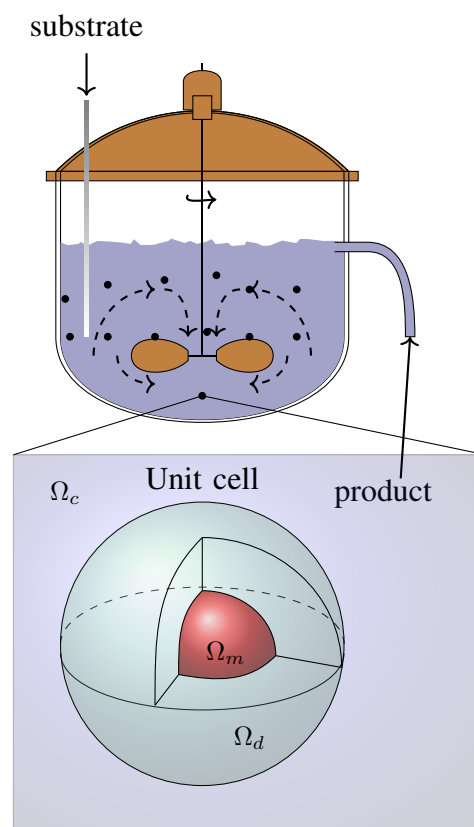


Figure 1. Continuous stirred tank reactor with enzyme-loaded microreactors (pellets) and a zoomed unit cell to be modelled.

Mathematical models have been widely used to investigate the kinetic peculiarities of the enzyme microreactors [8][13]. Models coupling the enzyme-catalysed reaction with the diffusion in enzyme microreactors are usually used. Since containing catalytic particles, the analyte in CSTR is well-stirred and set in powerful motion, the mass transport by diffusion outside the microreactors is usually neglected [15][16]. Mixing within CSTR creates the Nernst layer while increasing stirrer speed can reduce the thickness of Nernst layer. However, due to the inner force of attraction, the zero thickness of the diffusion shell (layer) can not be achieved [17]. We consider an array of identical spherical microreactors placed in the CSTR shown in Figure 1 [7], where area  $\Omega_m$  denotes a microreactor,  $\Omega_d$  denotes surrounding diffusion shell and  $\Omega_c$  is a convective region.

The goal of this work was to investigate the dependencies of the internal and external diffusion limitations on the yield and the effectiveness factors, modelled by reaction-diffusion equations, containing a non-linear term related to Michaelis-Menten kinetics [7][8][18]. The model involves three regions: the enzyme microreactor, where the enzyme reaction, as well as the mass transport by diffusion take place, a diffusion limiting region, where only the mass transport by diffusion takes place, and a convective region, where the constant analyte concentration is maintained. In practice, the laboratory experiments aimed to be performed with as small as possible particle layer size to avoid process limitations caused by diffusion of the reacting solution in the catalyst pore system. There is a practice of performing experiments under the fluid-dynamic conditions in order to eliminate the lack of mass transfer limitations outside the particles. However, it is not always possible to reduce the particle size as much as it is required for avoiding diffusion limitations.

It has been shown that for first order chemical reactions, the transient effectiveness factor depends not only on the Thiele modulus but also on the adsorption capacity of the system, the fact that should be taken into account when kinetic experiments are designed. However, the type of immobilization can raise the diffusion difference within the reactor and the Nernst layer. The porous materials as well as nanoparticles immobilized in microreactors, can be considered porous with respect to the Nernst layer. This paper also analyses how the porosity impacts effectiveness factor as well as the yield factor. Due to a strong non-linearity of the reaction term, the computer simulation was carried out using the finite difference technique [19].

The rest of the paper is organised as follows: in Section II, the mathematical model and microbioreactor characteristics are described; Section III formulates a dimensionless model and determines the main parameters of the bioreactor; Section IV describes the numerical model and the simulator; in Section V, the results of numerical experiments are presented, and conclusions close the article.

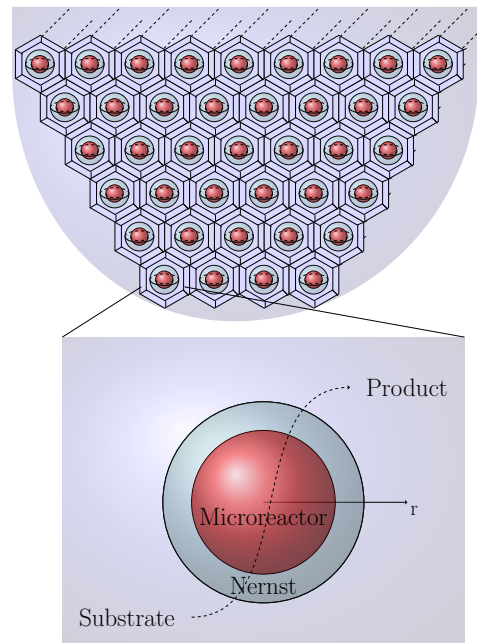
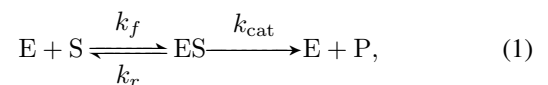


Figure 2. Principal structure of the unit cell consisting of a microbioreactor and the Nernst diffusion shell in homogeneously distributed volume.

## II. MATHEMATICAL MODEL

We consider an array of identical spherical microreactors placed in a continuous ideally stirred-tank reactor [7]. Assuming a uniform distribution of the microreactors (see Figure 2) in the tank and a comparably great distance between adjacent microreactors and fact that microreactor volume  $V_m$  is significantly smaller than the tank volume  $V$ , the spherical unit cell was modelled by an enzyme-loaded microreactor (pellet) and a surrounding diffusion shell (the Nernst diffusion layer). The principal structure of the tank containing uniformly distributed microreactors and a unit cell are presented in Figure 1, where  $\Omega_m$  denotes a microreactor (MR),  $\Omega_d$  stands for the diffusion shell and  $\Omega_c$  is a convective region.

In the enzyme-loaded MR layer we consider the enzyme-catalyzed reaction



the substrate (S) combines reversibly with an enzyme (E) to form a complex (ES). The complex then dissociates into the product (P) and the enzyme is regenerated [20][21]. The  $k_f$ ,  $k_r$  and  $k_{cat}$  are forward rate, reverse rate and catalytic rate constant, respectively.

Assuming the steady-state approximation, the concentration of the intermediate complex (ES) does not change and may be neglected when modelling the biochemical behaviour of the microreactor [7][21][22]. In the resulting scheme, the substrate (S) is enzymatically converted to the product (P),



### A. Governing Equations

Considering the symmetrical geometry of the microreactor and homogenised distribution of the immobilized enzyme inside the porous microreactor, the mathematical model can be described in one-dimensional domain using the radial distance [7].

Coupling enzymatic reaction in the microreactor (region  $\Omega_m$ ) with the one-dimensional-in-space diffusion, described by Fick's second law, and considering the steady-state of a system (2) leads to the following governing equations of the reaction-diffusion type ( $0 < r < R_0$ ):

$$D_{S,m} \frac{1}{r^2} \frac{d}{dr} \left( r^2 \frac{dS_m}{dr} \right) = \frac{V_{\max} S_m}{K_M + S_m}, \quad (3a)$$

$$D_{P,m} \frac{1}{r^2} \frac{d}{dr} \left( r^2 \frac{dP_m}{dr} \right) = -\frac{V_{\max} S_m}{K_M + S_m}, \quad (3b)$$

$r$  stands for space variable,  $S_m = S_m(r)$  and  $P_m = P_m(r)$  are the concentrations of the substrate and the reaction product in the microreactor, respectively,  $R_0$  is the radius of the microreactor,  $V_{\max} = k_{cat} E_0$  is the maximal enzymatic rate and  $K_M = (k_r + k_{cat})/k_f$  is the Michaelis constant. The volumetric reaction as a function from concentration is marked as  $V(S) = V_{\max} S_m / (K_M + S_m)$ .

In the Nernst diffusion layer  $\Omega_d$  only the mass transport by diffusion takes place ( $R_0 < r < R_1$ ):

$$D_{S,d} \frac{1}{r^2} \frac{d}{dr} \left( r^2 \frac{dS_d}{dr} \right) = 0, \quad (4a)$$

$$D_{P,d} \frac{1}{r^2} \frac{d}{dr} \left( r^2 \frac{dP_d}{dr} \right) = 0, \quad (4b)$$

$S_d = S_d(r)$  and  $P_d = P_d(r)$  are the concentrations of the substrate and the reaction product in the diffusion shell. Respectively,  $D_{S,d}$  and  $D_{P,d}$  are the diffusion coefficients of the materials in the bulk solution and  $R_1$  is the radius of the unit cell.

Microbioreactors are microparticles immobilized with the enzyme, so the core of the particle is porous. Due to the porosity of microbioreactor diffusion coefficients  $D_{S,m}$  and  $D_{P,m}$  can be expressed through diffusion coefficients for bulk solution [23],

$$D_{S,m} = \frac{D_{S,d} \epsilon_t}{\tau} \quad (5a)$$

$$D_{P,m} = \frac{D_{P,d} \epsilon_t}{\tau}, \quad (5b)$$

$\epsilon_t$  is porosity (void fraction space in a material) and  $\tau$  is tortuosity.

### B. Boundary Conditions

Fluxes of the substrate and the product through the stagnant external diffusion shell is assumed to be equal to the corresponding fluxes entering the surface of the microreactor,

$$\frac{\epsilon_t}{\tau} \frac{dS_m}{dr} \Big|_{r=R_0} = \frac{dS_d}{dr} \Big|_{r=R_0}, \quad (6a)$$

$$\frac{\epsilon_t}{\tau} \frac{dP_m}{dr} \Big|_{r=R_0} = \frac{dP_d}{dr} \Big|_{r=R_0}. \quad (6b)$$

The formal partition coefficient  $\phi$  is used to describe the specificity of concentration distribution of the compounds between two neighboring regions [7][24],

$$S_m(R_0) = \phi S_d(R_0), \quad (7a)$$

$$P_m(R_0) = \phi P_d(R_0). \quad (7b)$$

The partition within the reactor caused by porosity, so we assume that the porosity and partition coefficient is in a linear relationship:

$$\phi = \epsilon_t \quad (8)$$

Due to the symmetry of the microreactor, the zero-flux boundary conditions are defined for the center of the microreactor ( $r = 0$ ),

$$\frac{D_{S,d} \epsilon_t}{\tau} \frac{dS_m}{dr} \Big|_{r=0} = 0, \quad (9a)$$

$$\frac{D_{P,d} \epsilon_t}{\tau} \frac{dP_m}{dr} \Big|_{r=0} = 0. \quad (9b)$$

According to the Nernst approach, the shell of thickness  $\nu = R_1 - R_0$  remains unchanged with time [17][19]. Away from it, the solution is in motion and is uniform in concentration. Due to the continuous injection of the substrate into the stirred tank and washing off the product, the concentration in the convective region remains unchanged:

$$S_d(R_1) = S_0, \quad (10a)$$

$$P_d(R_1) = 0. \quad (10b)$$

The thickness  $\nu$  of the Nernst diffusion shell depends on the nature and stirring up of the buffer solution. Usually, more intensive stirring corresponds to the thinner diffusion layer (shell).

### C. Microbioreactor characteristics

In many industrial processes, especially in the production of low-value added products like biopesticides, bio-fertilizers, bio-surfactants ect. [10], it is important to continuously improve the yield and/or productivity of the reactor system [8]. The productivity is important, since this ensures an efficient utilization of the production capacity, i.e., the bioreactors.

The yield of the desired product on the substrate is one of the most important criteria for design and optimization of bioreactors. The economic feasibility of the process is expressed by the yield factor as the ratio of product formation rate and the substrate uptake rate [7][8].

The bioreactor construction is efficient enough when the product emission is relatively large with given substrate amount used. The product emission rate  $\bar{E}_{P,O}$  can be calculated by an integration of the product flux over the outer surface of the diffusion shell [8],

$$\begin{aligned}\bar{E}_{P,O} &= -\int_0^\pi \int_0^{2\pi} D_{P,d} \frac{dP_d}{dr} \Big|_{r=R_1} R_1^2 \sin(\theta) d\varphi d\theta \\ &= -4\pi R_1^2 D_{P,d} \frac{dP_d}{dr} \Big|_{r=R_1}.\end{aligned}\quad (11)$$

The product emission rate has the units of mol/s.

The substrate consumption rate  $\bar{C}_S$  over the whole microreactor can be calculated as follows:

$$\begin{aligned}\bar{C}_S &= \int_0^{R_0} \int_0^{2\pi} \int_0^\pi V(S) \sin(\theta) d\theta d\varphi r^2 dr \\ &= \int_0^{R_0} \int_0^{2\pi} 2V(S) d\varphi r^2 dr \\ &= 4\pi \int_0^{R_0} V(S) r^2 dr. \\ &= 4\pi \int_0^{R_0} \frac{V_{\max} S_m(r)}{K_M + S_m(r)} r^2 dr.\end{aligned}\quad (12)$$

The substrate emission rate also have the units of mol/s.

The yield factor  $\gamma$  for the microreactor system, as well as for the entire tank reactor shown in Figure 1, can be defined by the ratio of the product emission rate to the substrate consumption rate,

$$\gamma = \frac{\bar{E}_{P,O}}{\bar{C}_S}.\quad (13)$$

The yield factor is characterised by an actual rate within the reactor in contrast to the actual product formation rate.

The effectiveness factors characterise the interaction between action in microreactor in porous catalytic pellets and microreactors when particles are solid [25], and often used in the biochemical engineering [26][27]. The effectiveness factors are usually defined in terms of the stationary mode of biocatalytic systems [25][27][28]. The effectiveness factor  $\eta$  can be calculated [29]:

$$\begin{aligned}\eta &= \left( \frac{\bar{C}_S}{(4\pi R_0^3/3)} \right) / V(S_0) \\ &= \frac{3 \int_0^{R_0} V(S) r^2 dr}{R_0^3 V(S_0)} \\ &= \frac{3 \int_0^{R_0} \frac{V_{\max} S_m(r)}{K_M + S_m(r)} r^2 dr}{R_0^3 \frac{V_{\max} S_0}{K_M + S_0}}.\end{aligned}\quad (14)$$

Summarising definition (14), the effectiveness factor  $\eta$  can be defined also as the ratio of the average reaction rate actually observed in the MR to ideal rate evaluated at the bulk concentrations of the substrate [29][30].

### III. DIMENSIONLESS MODEL

In order to define the main governing parameters of the two compartment model (3)-(10), the dimensional variable  $r$

and unknown concentrations  $S_m(r), P_m(r), S_d(r), P_d(r)$  are replaced with the following dimensionless parameters:

$$\begin{aligned}\tilde{r} &= \frac{r}{R_0}, \quad \tilde{S}_m = \frac{S_m}{K_M} \\ \tilde{P}_m &= \frac{P_m}{K_M}, \quad \tilde{S}_d = \frac{S_d}{K_M}, \quad \tilde{P}_d = \frac{P_d}{K_M},\end{aligned}\quad (15)$$

$\tilde{r}$  is the dimensionless distance from the microreactor center and  $\tilde{S}_m(\tilde{r}), \tilde{P}_m(\tilde{r}), \tilde{S}_d(\tilde{r}), \tilde{P}_d(\tilde{r})$  are the dimensionless concentrations. Having defined dimensionless variables and unknowns, the following dimensionless parameters characterize the domain geometry and the substrate concentration in the bulk:

$$\tilde{\nu} = \frac{\nu}{R_0}, \quad \tilde{S}_0 = \frac{S_0}{K_M}, \quad D = \frac{\tau}{\epsilon_t}\quad (16)$$

$\tilde{\nu}$  is the dimensionless thickness of the Nernst diffusion layer,  $\tilde{S}_0$  is the dimensionless substrate concentration in the bulk solution,  $D$  is the dimensionless diffusion coefficient. The dimensionless thickness of the microreactor equals one.

#### A. Model description

The governing equations (3) in the dimensionless coordinates are expressed as follows ( $0 < \tilde{r} < 1$ ):

$$\frac{1}{\tilde{r}^2} \frac{d}{d\tilde{r}} \left( \tilde{r}^2 \frac{d\tilde{S}_m}{d\tilde{r}} \right) - \sigma^2 \frac{\tilde{S}_m}{1 + \tilde{S}_m} = 0,\quad (17a)$$

$$\frac{1}{\tilde{r}^2} \frac{d}{d\tilde{r}} \left( \tilde{r}^2 \frac{d\tilde{P}_m}{d\tilde{r}} \right) + \sigma^2 \frac{\tilde{S}_m}{1 + \tilde{S}_m} = 0,\quad (17b)$$

$\sigma$  is the Thiele modulus or the Damköhler number [8][31][32] defined as:

$$\sigma^2 = \frac{V_{\max} R_0^2}{K_M D_{S,m}} = \frac{V_{\max} R_0^2 \tau}{K_M D_{S,d} \epsilon_t}.\quad (18)$$

The governing equations (4) take the following form ( $1 < \tilde{r} < 1 + \tilde{\nu}$ ):

$$D \frac{1}{\tilde{r}^2} \frac{d}{d\tilde{r}} \left( \tilde{r}^2 \frac{d\tilde{S}_d}{d\tilde{r}} \right) = 0,\quad (19a)$$

$$D \frac{1}{\tilde{r}^2} \frac{d}{d\tilde{r}} \left( \tilde{r}^2 \frac{d\tilde{P}_d}{d\tilde{r}} \right) = 0.\quad (19b)$$

The matching conditions (6)-(10) become:

$$\frac{d\tilde{S}_m}{d\tilde{r}} \Big|_{\tilde{r}=1} = D \frac{d\tilde{S}_d}{d\tilde{r}} \Big|_{\tilde{r}=1}\quad (20a)$$

$$\frac{d\tilde{P}_m}{d\tilde{r}} \Big|_{\tilde{r}=1} = D \frac{d\tilde{P}_d}{d\tilde{r}} \Big|_{\tilde{r}=1},\quad (20b)$$

$$\tilde{S}_m(1) = \phi \tilde{S}_d(1),\quad (21a)$$

$$\tilde{P}_m(1) = \phi \tilde{P}_d(1),\quad (21b)$$

$$\frac{d\tilde{S}_m}{d\tilde{r}} \Big|_{\tilde{r}=0} = 0,\quad (22a)$$

$$\frac{d\tilde{P}_m}{d\tilde{r}} \Big|_{\tilde{r}=0} = 0,\quad (22b)$$

$$\tilde{S}_d(1 + \tilde{\nu}) = \tilde{S}_0, \quad (23a)$$

$$\tilde{P}_d(1 + \tilde{\nu}) = 0. \quad (23b)$$

### B. Model reduction

The second order homogeneous differential equations (19) can be easily integrated ( $1 < \tilde{r} < 1 + \tilde{\nu}$ ) [19],

$$\tilde{S}_d(\tilde{r}) = \frac{c_1}{\tilde{r}} + c_2, \quad \tilde{P}_d(\tilde{r}) = \frac{d_1}{\tilde{r}} + d_2, \quad (24)$$

$c_1$ ,  $c_2$ ,  $d_1$  and  $d_2$  are constants of integration. By evaluating the integration constants from the boundary conditions (20) and (23), we get the following solution to the system (19):

$$\tilde{S}_d(\tilde{r}) = \tilde{S}_0 - \frac{\epsilon_t}{\tau} \left( \frac{1}{\tilde{r}} - \frac{1}{1 + \tilde{\nu}} \right) \frac{d\tilde{S}_m}{d\tilde{r}} \Big|_{r=1}, \quad (25a)$$

$$\tilde{P}_d(\tilde{r}) = -\frac{\epsilon_t}{\tau} \left( \frac{1}{\tilde{r}} - \frac{1}{1 + \tilde{\nu}} \right) \frac{d\tilde{P}_m}{d\tilde{r}} \Big|_{r=1}. \quad (25b)$$

After applying the obtained expressions (25), the matching conditions (21) can be expressed as the flux boundary conditions,

$$\frac{d\tilde{S}_m}{d\tilde{r}} \Big|_{\tilde{r}=1} = \beta_S \left( \tilde{S}_0 - \frac{\tilde{S}_m(1)}{\phi} \right), \quad (26a)$$

$$\frac{d\tilde{P}_m}{d\tilde{r}} \Big|_{\tilde{r}=1} = \beta_P \left( -\frac{\tilde{P}_m(1)}{\phi} \right), \quad (26b)$$

$\beta_S$  and  $\beta_P$  are the Biot numbers for the substrate and the product [33][34], respectively.

$$\begin{aligned} \beta_S &= \frac{D_{S,d}}{D_{S,d}\epsilon_t} \frac{1 + \tilde{\nu}}{\tilde{\nu}} = \frac{D_{S,d}R_1}{D_{S,d}\epsilon_t(R_1 - R_0)} \\ \beta_P &= \frac{D_{P,d}}{D_{P,d}\epsilon_t} \frac{1 + \tilde{\nu}}{\tilde{\nu}} = \frac{D_{P,d}R_1}{D_{P,d}\epsilon_t(R_1 - R_0)} \\ \beta &= \beta_S = \beta_P = \frac{\tau}{\epsilon_t} \frac{1 + \tilde{\nu}}{\tilde{\nu}} = D \frac{R_1}{(R_1 - R_0)}. \end{aligned} \quad (27)$$

The boundary value problem (17)-(23) has been reduced to the boundary value problem described by the governing equations (17), the boundary condition (22) and the flux boundary condition (26).

### C. Governing parameters

The initial set of model parameters has been reduced to the following aggregate dimensionless parameters:  $\tilde{\nu}$  is the relative thickness of the Nernst diffusion layer,  $\sigma$  is the diffusion module,  $\beta$  is the Biot number,  $\tilde{S}_0$  is the substrate concentration in the bulk,  $\phi$  is the formal partition coefficient.

The dimensionless factor  $\sigma^2$  essentially compares the rate of enzyme reaction ( $V_{\max}/K_M$ ) with the diffusion through the enzyme-loaded microreactor ( $D_{S,m}/R_0^2$ ). If  $\sigma^2 \ll 1$ , the

enzyme kinetics controls the bioreactor action. The action is under diffusion control when  $\sigma^2 \gg 1$ .

The Biot number indicates the internal mass transfer resistance to the external one [33][34]. When the Biot number is small, the effect of the external diffusion is the most marked. As the Biot number increases, the effect of the external diffusion becomes less important.

The diffusion module and the Biot number are widely used in analysis and design of different bioreactors [34]. The experiment conducted by Kont et al. [11] proved the external mass-transfer limitations to be negligible for the Biot number greater than one using the first order kinetics model of CSTR and packed-bed reactors (PBR), which corresponds condition (10). Typically, designers seek for bioreactors acting in the reaction-limited regime, since in this case reaction and diffusion occur on different time scales [35].

### D. Limiting cases

Analytical solutions of product and substrate concentrations can be found for the limiting cases when volumetric reactions become zero or first kinetics [7][33]. Analytical solutions have practical value, the models when diffusion is not fixed and depends on porosity and tortuosity are rarely analyzed (see equation (5)).

*Zero order kinetics:* When the substrate concentration  $S_0$  is very high compared to the Michaelis constant  $K_M$  ( $S_0 \gg K_M$ ), the reaction term reduces to the zero order reaction rate  $V_{\max}$ , then volumetric reactions becomes  $V(S) \approx V_{\max}$ .

The solution of substrate and product concentrations with the boundary conditions (6)-(10) gives the following expressions:

$$S_m(r) = \phi S_0 - \frac{V_{\max}\tau}{6D_{S,d}\epsilon_t} \left( R_0^2 - r^2 + \frac{2\phi R_0^2}{\beta} \right) \quad (28)$$

$$P_m(r) = \frac{V_{\max}\tau}{6D_{P,d}\epsilon_t} \left( R_0^2 - r^2 + \frac{2\phi R_0^2}{\beta} \right) \quad (29)$$

$$S_d(r) = S_0 - \frac{V_{\max}R_0^3}{3D_{S,d}} \left( \frac{1}{r} - \frac{1}{R_1} \right) \quad (30)$$

$$P_d(r) = \frac{V_{\max}R_0^3}{3D_{P,d}} \left( \frac{1}{r} - \frac{1}{R_1} \right) \quad (31)$$

**Corollary 1.** *The yield and effectiveness factors are equal to one for zero order kinetics.*

$$\begin{aligned} \bar{E}_{P,O}^0 &= -4\pi R_1^2 D_{P,d} \frac{dP_d}{dr} \Big|_{r=R_1} \\ &= -4\pi R_1^2 D_{P,d} \frac{(-1)}{3} R_0^3 \frac{V_{\max}}{D_{P,d}R_1^2} \\ &= \frac{4}{3}\pi R_0^3 V_{\max} \\ \bar{C}_S^0 &= \frac{4}{3}\pi R_0^3 V_{\max} \\ \gamma^0 &= \frac{\bar{E}_{P,O}^0}{\bar{C}_S^0} = 1 \end{aligned} \quad (32)$$

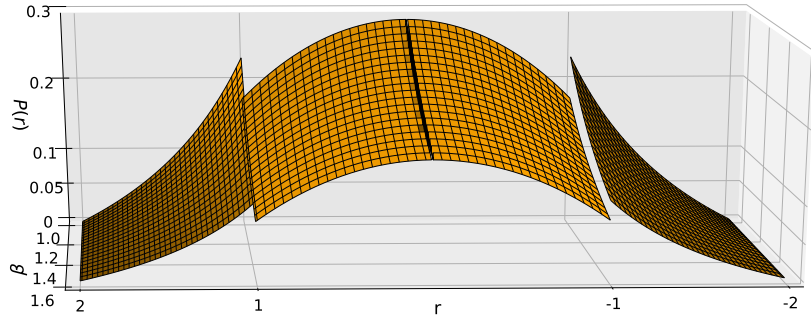


Figure 3. Concentration profiles of the product concentration in the microreactor (simulated at the substrate concentration  $\tilde{S}_0 = 1$  porosity  $\epsilon_t = 0.75$  and different values of the Biot number  $\beta \in [1, 1.6]$ , the other parameters are as defined in (40)).

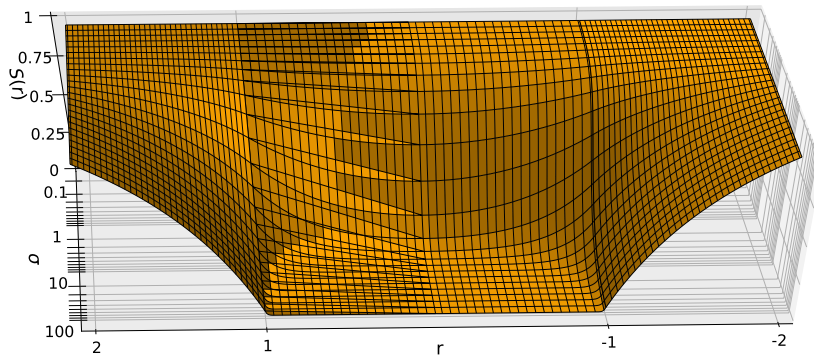


Figure 4. Concentration profiles of the substrate concentration in the microreactor (simulated at the substrate concentration  $\tilde{S}_0 = 1$ , porosity  $\epsilon_t = 1$  and different values of the Thiele module  $\sigma \in [10^{-1}, 10^2]$ , the other parameters are as defined in (40)).

$$\eta^0 = \frac{3 \int_0^{R_0} V_{\max} r^2 dr}{R_0^3 V_{\max}} = 1 \quad (33)$$

equations (3) reduces to the first order reaction rate, then volumetric reactions becomes  $V(S) \approx V_{\max} S / K_M$ .

The zero order kinetics rate does not depend on the concentration profiles, so, naturally, such type of system is efficient.

The solution of substrate and product concentrations with the boundary conditions (6)-(10) at first order kinetics gives the following expressions:

*First order kinetics:* At such low concentration of the substrate as  $S_0 \ll K_M$ , the non-linear reaction rate in

$$S_m(r) = \frac{\phi S_0 R_1 R_0 \tau / \epsilon \sinh(mr)}{r(\tau / \epsilon R_1 \sinh(\sigma) + \phi(R_1 - R_0)(\sigma \cosh(\sigma) - \sinh(\sigma)))}, \quad (34)$$

$$S_d(r) = \frac{S_0 R_1 (\tau / \epsilon r \sinh(\sigma) + \phi(r - R_0)(\sigma \cosh(\sigma) - \sinh(\sigma)))}{r(\tau / \epsilon R_1 \sinh(\sigma) + \phi(R_1 - R_0)(\sigma \cosh(\sigma) - \sinh(\sigma))} \quad (35)$$

$0 \leq r \leq R_0.$

$$P_m(r) = -\left( \phi S_0 (R_1 \phi \sigma \cosh(\sigma)r - R_0 \phi \sigma \cosh(\sigma)r - \sinh(mr)R_0 R_1 D^* \tau / \epsilon - R_1 \phi \sinh(\sigma)r + R_1 \sinh(\sigma)D^* \tau / \epsilon r + R_0 \phi \sinh(\sigma)r) \right) / \left( m^2 r (\tau / \epsilon R_1 \sinh(\sigma) + \phi(R_1 - R_0)(\sigma \cosh(\sigma) - \sinh(\sigma))) D^* \right), \quad (36)$$

$$P_d(r) = -\frac{\phi S_0 R_0 (R_1 - r)(\sigma \cosh(\sigma) - \sinh(\sigma))}{m^2 r (\tau / \epsilon R_1 \sinh(\sigma) + \phi(R_1 - R_0)(\sigma \cosh(\sigma) - \sinh(\sigma))) D^*} \quad (37)$$

$R_0 \leq r \leq R_1.$



**Corollary 2.** *The yield and effectiveness factors have the following form at first order kinetics.*

$$\gamma^1 = \sigma^2, \quad (38)$$

$$\eta^1 = \frac{3\beta\phi(\sigma \coth \sigma - 1)}{\sigma^2(\beta + \phi(\sigma \coth \sigma - 1))}. \quad (39)$$

One can see that the effectiveness coefficient lies in the interval  $[0, 1]$ , while yield can grow. However, in practical applications  $\sigma \ll 1$ .

#### IV. DIGITAL SIMULATION OF EXPERIMENTS

The non-linearity of the governing equations prevents us from solving the boundary value problem (17)-(23) analytically, hence the numerical model was constructed and solved using finite difference technique [19]. An explicit scheme was used; however, due to Michaelis-Menten non-linearity, further construction of equations was used:

$$D_{C,m} \cdot \frac{1}{r^2} \frac{d}{dr} \left( r^2 \frac{dC_m^n}{dr} \right) = \pm \frac{V_{\max} C_m^n}{K_M + C_m^{n-1}},$$

$C = S, P$ . Tridiagonal matrix was constructed from the equations. In the numerical simulation, the scheme was run until the following loss became very small:

$$\mathcal{L} = \|S^n - S^{n-1}\|_{l^2} + \|P^n - P^{n-1}\|_{l^2} < \epsilon,$$

decay rate value  $\epsilon = 10^{-14}$  was used over  $l^2$  norm. An explicit scheme of finite difference was built on a uniform discrete grid with 128 points in space direction [18]. The simulator has been programmed by the authors in C++ language [36].

The numerical solution of the mathematical model (17)-(23) was validated by using the exact analytical solutions known for very special cases of the model parameters [7][18][31][34] see equations (28)-(37).

#### V. RESULTS AND DISCUSSION

To investigate the effects of the geometry and catalytic activity of the microreactor, the reactor action was simulated and the yield and the effectiveness factor was calculated for very different values of the Biot number  $\beta$ , the Thiele module  $\sigma$ , the substrate dimensionless concentration  $S_0$ , the porosity  $\epsilon_t$ .

##### A. Concentration profiles

Figure 3 shows the profiles of the product concentration  $P$  calculated from the microreactor model (17)-(23) changing the Biot number  $\beta$  and the porosity equal  $\epsilon_t = 0.75$ . Figure 4 shows the profiles of the substrate concentration  $S$  changing the Thiele module  $\sigma$  and the porosity  $\epsilon_t = 1$ . As both figures demonstrate, the following parameters of the model remain unchanged:

$$D_{S,d} = D_{P,d}, \quad \beta = 1, \quad \tilde{\nu} = 1. \quad (40)$$

One can be seen in Figure 4, where low Thiele modulus values  $\sigma < 1$ , which indicates that the species pass the Nerst

diffusion layer fast, allow the concentrations approach the straight line because of linearity of governing equations in the area  $\tilde{r} \in (1, 1 + \tilde{\nu})$ . On the other hand, high Thiele modulus values ( $\sigma \geq 100$ ) (see Figure 3) lead to significant differences in concentration distribution across the outer boundary of the microreactor. Both the radius of dimensionless microreactor and the Nerst layer thickness is equal to one.

##### B. The impact of the Biot number, Thiele module and substrate concentration

To investigate the dependence of the yield factor  $\gamma$ , the effectiveness factor  $\eta$  on the Biot number  $\beta$ , changing the Biot number in a range of  $[1, 10^2]$ , the factor  $\gamma$  was calculated at different values of the Thiele module  $\sigma$  in a range of  $[10^{-1}, 10^2]$  and the substrate concentration  $\tilde{S}_0$  was calculated in a range of  $[10^{-3}, 10^3]$ .

*Impact of the Biot number:* The results of the calculations of yield factor  $\gamma$  when Biot number  $\beta$  and Thiele module  $\sigma$  is changing and the porosity  $\epsilon_t = 0.1, 0.5, 1$  are depicted in Figure 5.

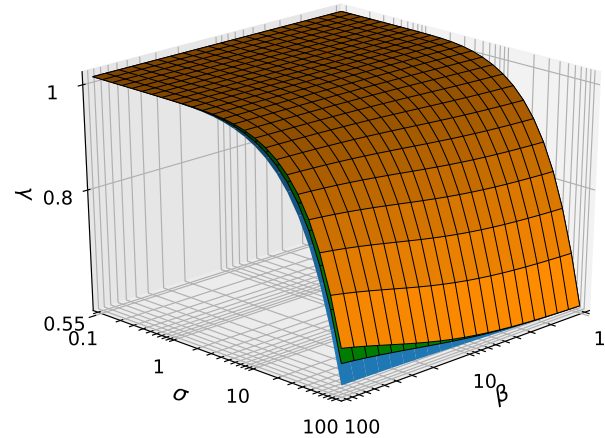


Figure 5. The yield factor  $\gamma$  vs. Biot number  $\beta$  and Thiele module  $\sigma$  at porosity  $\epsilon_t$ : 0.1, 0.5, 1, the other parameters are as in (40).

In Figure 5, the yield factor  $\gamma$  is presented when concentration  $\tilde{S}_0$  is equal to one. It is apparent that maximal efficiency can be achieved only with Thiele module  $\sigma < 1$ . It is worth to mention that porosity can be considered as neglected for yield factor. With large values of Thiele module, the yield factor  $\gamma$  is nearing to zero independently of the porosity  $\epsilon_t$  or  $\beta$ . The yield factor  $\gamma$ , practically, does not depend on  $\beta$  for  $\sigma < 1$ .

The Biot number and substrate concentration is neglected to yield factor  $\gamma$  with Thiele module  $\sigma < 20$ . On the other hand, the Nerst diffusion layer may be neglected when the Biot number is higher than approximately 20 [34][37].

*Impact of the substrate concentration:* Calculation results of the yield factor  $\gamma$  when substrate concentration  $S_0$  and Thiele module  $\sigma$  is changing and the porosity  $\epsilon_t = 0.1, 0.5, 1$  are depicted in Figure 6.

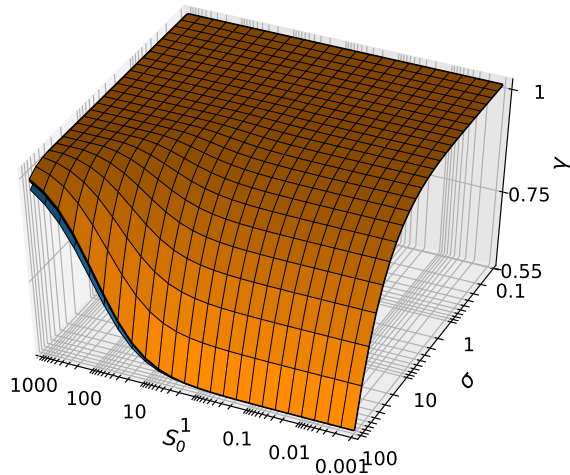


Figure 6. The yield factor  $\gamma$  vs. Thiele module  $\sigma$  and initial concentration  $S_0$  at porosity  $\epsilon_t$ : 0.1, 0.5, 1, the other parameters are as in (40).

One can see (Figure 6) a non-linear impact of the substrate concentration on the yield factor. As a function of  $\tilde{S}_0$ , the yield factor  $\gamma$  is a monotonously increasing function with the limit of one. At high values of the Thiele module  $\sigma > 20$ , the yield factor is decreasing to zero near low values of substrate (see Figure 6). The yield factor, limiting value of one, can be reached with the low Thiele module values  $\sigma < 20$ .

The yield factor  $\gamma$  is, practically, invariant to changes in the substrate concentration  $\tilde{S}_0$  when the Michaelis-Menten kinetics approach the first order ( $\tilde{S}_0 \ll 1$ ) or zero order kinetics ( $\tilde{S}_0 \gg 1$ ). In intermediate values of  $\tilde{S}_0$ , when the kinetics changes from the first to zero order, the yield factor  $\gamma$  noticeably increases with increasing the substrate concentration at low Thiele module values.

**Impact of the Thiele Module:** It can be seen in Figure 5 and Figure 6 that the yield factor  $\gamma$ , practically, does not depend on  $\sigma$  and approaches to one when the bioreactor acts notably under the bioreaction control ( $\sigma < 20$ ). At mixed conditions when the diffusion action is influenced by both the enzyme kinetics and the diffusion, the yield factor  $\gamma$  noticeably decreases decreasing the substrate concentration  $S_0$ . Figure 6 also shows that the factor  $\gamma$  increases while increasing the substrate concentration (as in Figure 6) as well as when increasing the Biot number  $\beta$  (as in Figure 5).

**C. Impact of the porosity**

To investigate the dependence of the yield factor  $\gamma$ , the effectiveness factor  $\eta$  on porosity  $\epsilon_t$ , the calculations were performed in a range of [0.1, 1]. The ranges of Thiele module  $\sigma$ , Biot number  $\beta$  and tortuosity was used as in the previous Section.

Figure 7 shows the effectiveness factor  $\eta$  as an increasing function of the porosity  $\epsilon_t$  when Thiele module is one and Biot number is two. When the Michaelis-Menten kinetics approaches the first order ( $\tilde{S}_0 \ll 1$ ), the effectiveness factor  $\eta$  becomes a linear function from the porosity. The effectiveness factor  $\eta$  approaches one as increased concentrations are becoming zero order kinetics ( $\tilde{S}_0 \gg 1$ ). Those limits can be

validated from calculated factors at zero order (33) and the first order kinetics (39).

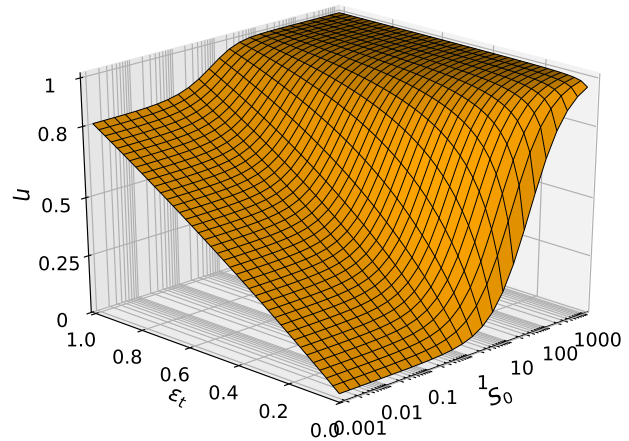


Figure 7. The effectiveness factor  $\eta$  vs. initial concentration  $S_0$  and porosity  $\epsilon_t$ , the other parameters are as in (40).

Figure 8 shows the effectiveness factor  $\eta$  as an increasing function of the porosity  $\epsilon_t$  when Thiele module and concentrations are equal to one. The effectiveness factor  $\eta$ , practically, does not depend on the Biot number for  $\beta > 2$  and increases with increasing the porosity and the Biot number.

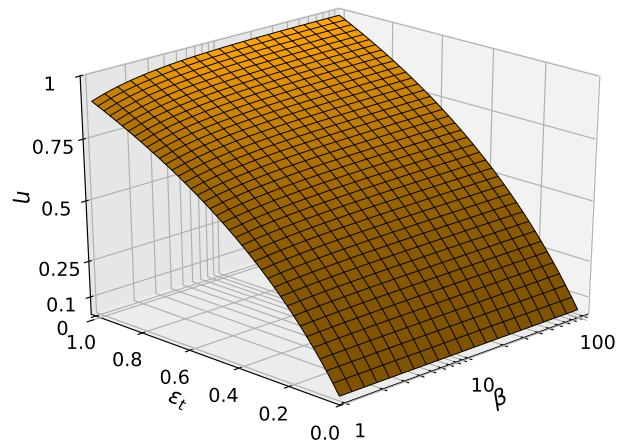


Figure 8. The effectiveness factor  $\eta$  vs. Biot number  $\beta$  and porosity  $\epsilon_t$ , the other parameters are as in (40).

Figure 9 shows the yield  $\gamma$  as an increasing function of the porosity  $\epsilon_t$  when concentrations are equal to one and the Biot number is two. It is evident that high Thiele module values  $\sigma \gg 10$  are significantly decreasing any efficiency of the system and the yield factor practically does not depend on the porosity  $\epsilon_t$ . On the other hand, the small Thiele module values give a linear dependency from the porosity. It can be noted that yield as a function of Thiele module is nonlinear and increases with decreasing diffusion module.



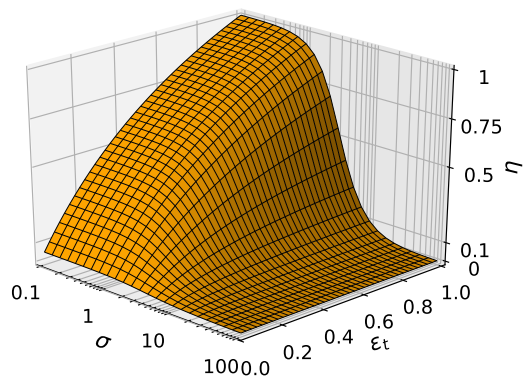


Figure 9. The effectiveness factor  $\eta$  vs. the Thiele module  $\sigma$  and porosity  $\epsilon_t$ , the other parameters are as in (40).

Figure 10 shows the yield  $\gamma$  as an increasing function of the Thiele module and practically does not depend on the porosity  $\epsilon_t$  when Thiele module is one and the Biot number is two.

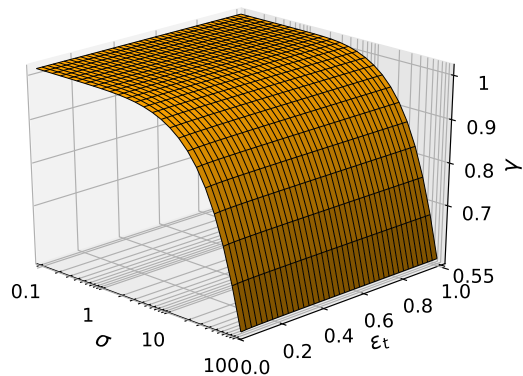


Figure 10. The yield factor  $\gamma$  vs. the Thiele module  $\sigma$  and porosity  $\epsilon_t$ , the other parameters are as in (40).

## VI. CONCLUSION AND FUTURE WORK

The mathematical model (3)-(10) and the corresponding dimensionless model (15)-(23) of the microbioreactor can be successfully used to investigate the behaviour of the catalytic microreactor and to optimize its configuration.

The yield of the product increases with increasing the substrate concentration (Figure 6) and with decreasing the Thiele module (Figure 5). However, the effectiveness of the yield factor can be achieved to the limit of one, with not high Thiele module value  $\sigma < 20$ . More importantly, the yield factor, practically, does not depend on the Biot number (Figure 5) and the porosity (Figure 10).

The increase in the substrate concentration becomes ineffective when the enzyme reaction is under control of reaction control  $\sigma < 20$  (Figure 6). The high yield can be achieved

only when the enzyme kinetics controls the bioreactor action  $\sigma < 20$  (Figure 6).

The transient effectiveness factor is an increasing function of porosity and, practically, does not depend on the Biot number (Figure 8). However, strong non-linear dependencies appear when analysing the impact of porosity and Thiele module (Figure 9). Also, is evident that the effectiveness factor approach zero under diffusion control  $\sigma > 10$  and is limited of porosity under action control  $\sigma < 0.1$ . The dependency from substrate concentration (Figure 7) also shows a non-linear relationship. The effectiveness increases to one with increase in the substrate concentration and reduces to the linear function of porosity when  $S_0 < 0.01$ .

Such formulation can be useful to find the optimal parameters of such biosystem construction [12]. More importantly, it might improve the design and production of microbioreactors.

There are some limitations worth to mention that might be used for the future investigations. First of all, in physical experiments, pellets can not be considered as the perfect spheres, which requires the modelling of more sophisticated domains in 2D and 3D spaces. Secondly, the system with time dependent characteristics should be considered in the future work.

## REFERENCES

- [1] L. Petkevicius and R. Baronas, "Numerical Simulation and Analysis of Enzyme-Catalysed Substrate Conversion in a Microbioreactor," in *SIMUL 2017: The Ninth International Conference on Advances in System Simulation*. IARIA, 2017, pp. 1–6.
- [2] A. Regalado-Méndez, R. R. Romero, R. N. Rangel, and S. Skogestad, "Biodiesel Production in Stirred Tank Chemical Reactors: A Numerical Simulation," in *New Trends in Networking, Computing, E-learning, Systems Sciences, and Engineering*. Springer, 2015, pp. 109–116.
- [3] O. N. Ağdağ and D. T. Sponza, "Anaerobic/aerobic treatment of municipal landfill leachate in sequential two-stage up-flow anaerobic sludge blanket reactor (UASB)/completely stirred tank reactor (CSTR) systems," *Process Biochemistry*, vol. 40, no. 2, pp. 895–902, 2005.
- [4] A. Miyawaki, S. Taira, and F. Shiraishi, "Performance of continuous stirred-tank reactors connected in series as a photocatalytic reactor system," *Chemical Engineering Journal*, vol. 286, pp. 594–601, 2016.
- [5] M. A. Dareioti and M. Kornaros, "Effect of hydraulic retention time (HRT) on the anaerobic co-digestion of agro-industrial wastes in a two-stage CSTR system," *Bioresour Technol*, vol. 167, pp. 407–415, 2014.
- [6] A. J. Straathof and P. Adlercreutz, *Applied Biocatalysis*. CRC Press, 2000.
- [7] P. M. Doran, *Bioprocess Engineering Principles*. Academic Press, 1995.
- [8] J. Villadsen, J. Nielsen, and G. Liden, *Bioreaction Engineering Principles*. Dordrecht: Springer, 2011.
- [9] S. K. Dubey, A. Pandey, and R. S. Sangwan, *Current Developments in Biotechnology and Bioengineering: Crop Modification, Nutrition, and Food Production*. Elsevier, 2016.
- [10] J. W. Wong, R. D. Tyagi, and A. Pandey, *Current Developments in Biotechnology and Bioengineering: Solid Waste Management*. Elsevier, 2016.
- [11] A. Konti, D. Mamma, D. G. Hatzinikolaou, and D. Kekos, "3-Chloro-1, 2-propanediol biodegradation by Ca-alginate immobilized *Pseudomonas putida* DSM 437 cells applying different processes: mass transfer effects," *Bioprocess and Biosystems Engineering*, vol. 39, no. 10, pp. 1597–1609, 2016.
- [12] D. Caşcaval, A. C. Blaga, and A.-I. Galaction, "Diffusional effects on anaerobic biodegradation of pyridine in a stationary basket bioreactor with immobilized *Bacillus* spp. cells," *Environmental Technology*, pp. 1–13, 2017.

- [13] R. Karande, A. Schmid, and K. Buehler, "Applications of multiphase microreactors for biocatalytic reactions," *Organic Process Research & Development*, vol. 20, no. 2, pp. 361–370, 2016.
- [14] K. F. Jensen, "Flow chemistry—microreaction technology comes of age," *AIChE Journal*, vol. 63, no. 3, pp. 858–869, 2017.
- [15] F. M. Pereira and S. C. Oliveira, "Occurrence of dead core in catalytic particles containing immobilized enzymes: analysis for the michaelis-menten kinetics and assessment of numerical methods," *Bioprocess and Biosystems Engineering*, vol. 39, no. 11, pp. 1717–1727, 2016.
- [16] M. B. Kerby, R. S. Legge, and A. Tripathi, "Measurements of kinetic parameters in a microfluidic reactor," *Analytical Chemistry*, vol. 78, no. 24, pp. 8273–8280, 2006.
- [17] J. Wang, *Analytical Electrochemistry*, 3rd ed. Hoboken, New Jersey: John Wiley & Sons, 2006.
- [18] R. Baronas, F. Ivanauskas, and J. Kulys, *Mathematical Modeling of Biosensors*. Dordrecht: Springer, 2010. [Online]. Available: <http://www.springer.com/chemistry/book/978-90-481-3242-3>
- [19] D. Britz and J. Strutwolf, *Digital Simulation in Electrochemistry*, 4th ed., ser. Monographs in Electrochemistry. Cham: Springer, 2016.
- [20] M. F. Chaplin and C. Bucke, "The large-scale use of enzymes in solution," *Enzyme Technology*, pp. 138–166, 1990.
- [21] H. Gutfreund, *Kinetics for the Life Sciences*. Cambridge: Cambridge University Press, 1995.
- [22] L. A. Segel and M. Slemrod, "The quasi-steady-state assumption: a case study in perturbation," *SIAM Rev.*, vol. 31, no. 3, pp. 446–477, 1989.
- [23] P. Grathwohl, *Diffusion in natural porous media: contaminant transport, sorption/desorption and dissolution kinetics*. Springer Science & Business Media, 2012, vol. 1.
- [24] M. Velkovsky, R. Snider, D. E. Cliffler, and J. P. Wikswa, "Modeling the measurements of cellular fluxes in microreactor devices using thin enzyme electrodes," *J. Math. Chem.*, vol. 49, no. 1, pp. 251–275, 2011.
- [25] L. A. Belfiore, *Transport Phenomena for Chemical Reactor Design*. Hoboken, New Jersey: John Wiley & Sons, 2003.
- [26] D. D. Do and P. F. Greenfield, "The concept of an effectiveness factor for reaction problems involving catalyst deactivation," *Chem. Eng. J.*, vol. 27, no. 2, pp. 99–105, 1983.
- [27] P. M. Doran, *Bioprocess Engineering Principles*, 2nd ed. Waltham, MA: Academic Press, 2013.
- [28] P. Harriott, *Chemical Reactor Design*. New York: Marcel Dekker, 2003.
- [29] H. J. Vos, P. J. Heederik, J. J. M. Potters, and K. C. A. M. Luyben, "Effectiveness factor for spherical biofilm catalysts," *Bioprocess Eng.*, vol. 5, no. 2, pp. 63–72, 1990.
- [30] T. Schulmeister, "Mathematical modelling of the dynamic behaviour of amperometric enzyme electrodes," *Sel. Electrode Rev.*, vol. 12, pp. 203–260, 1990.
- [31] ———, "Mathematical modelling of the dynamic behaviour of amperometric enzyme electrodes," *Selective Electrode Reviews*, vol. 12, no. 2, pp. 203–260, 1990.
- [32] D. J. Fink, T. Na, and J. S. Schultz, "Effectiveness factor calculations for immobilized enzyme catalysts," *Biotechnology and Bioengineering*, vol. 15, no. 5, pp. 879–888, 1973.
- [33] R. Aris, *Mathematical Modeling: a Chemical Engineer's Perspective*. Academic Press, 1999, vol. 1.
- [34] M. E. Davis and R. J. Davis, *Fundamentals of chemical reaction engineering*. New York: McGraw-Hill, 2003.
- [35] D. A. Edwards, B. Goldstein, and D. S. Cohen, "Transport effects on surface-volume biological reactions," *J. Math. Biol.*, vol. 39, no. 6, pp. 533–561, 1999.
- [36] W. T. Vetterling, *Numerical Recipes Example Book (C++): The Art of Scientific Computing*. Cambridge University Press, 2002.
- [37] R. Baronas, "Nonlinear effects of diffusion limitations on the response and sensitivity of amperometric biosensors," *Electrochimica Acta*, vol. 240, pp. 399–407, 2016.